Direct observation of apical oxygen vacancies in the high-temperature superconductor $YBa_2Cu_3O_{7-x}$

Steven T. Hartman,[1,*] Bernat Mundet,[2,*] Juan-Carlos Idrobo,[3] Xavier Obradors,[2] Teresa Puig,[2] Jaume Gázquez,[2,†] and Rohan Mishra[4,1,‡]

[1]*Institute of Materials Science and Engineering, Washington University in St. Louis, St. Louis, Missouri 63130, USA*
[2]*Institut de Ciéncia de Materials de Barcelona (ICMAB-CSIC), Campus UAB, Bellaterra, 08193 Barcelona, Spain*
[3]*Center for Nanophase Materials Sciences, Oak Ridge National Laboratory, Oak Ridge, Tennessee 37831, USA*
[4]*Department of Mechanical Engineering and Materials Science, Washington University in St. Louis, St. Louis, Missouri 63130, USA*

(Received 3 April 2019; revised manuscript received 27 September 2019; published 22 November 2019)

The properties of the high-temperature superconductor $YBa_2Cu_3O_{7-x}$ (YBCO) depend on the concentration of oxygen vacancies (V_O). It is generally agreed upon that V_O form in the CuO chains, even at low concentrations where the critical temperature for superconductivity peaks ($x \approx 0.07$), with only a handful of reports suggesting the presence of V_O at the apical sites. In this paper, we show direct evidence of apical V_O in optimally doped YBCO samples. Using density-functional-theory calculations, we predict that isolated V_O are equally favorable to form in either the CuO chains or the apical sites, which we confirm using atomic-resolution scanning transmission electron microscope imaging and spectroscopy. We further show that apical V_O lead to significant lattice distortions and changes in the electronic structure of YBCO, indicating they should be considered on an equal footing with chain V_O to understand the superconducting properties of YBCO in the optimal doping region.

DOI: 10.1103/PhysRevMaterials.3.114806

I. INTRODUCTION

Subtle changes in structure and stoichiometry stemming from defects influence many functional properties of ceramics. A paradigmatic example is the high-temperature superconductor $YBa_2Cu_3O_{7-x}$ (YBCO), where its critical temperature (T_c) and critical current density (J_c) are governed by oxygen vacancies (V_O) [1–3]. The structure of YBCO, shown in Fig. 1(a), is that of an oxygen-deficient perovskite. Oxygen is absent from the Y layers, and from half of the sites in the CuO layers present between two BaO layers, which are commonly referred to as CuO chains [4]. The bridging oxygen in these chains can also be removed under reducing conditions, allowing the stoichiometry to vary continuously from $YBa_2Cu_3O_7$ to $YBa_2Cu_3O_6$. Chain V_O leads to structural distortions in their vicinity and dopes the system with electrons [1]. Optimal doping, at $x = 0.07$, gives a maximum T_c of 92 K, while $x > 0.55$, destroys the superconducting state [1], thus controlling the oxygen stoichiometry allows a way to tune T_c. J_C is also modulated by the oxygen content, since the magnetic vortex pinning is sensitive to both the carrier concentration and the distortions around V_O [2,3,5].

Oxygen vacancies have received enormous attention, but nearly all past studies have focused on the chain V_O, O(1) in Fig. 1(a). There are three other oxygen sites in YBCO, one apical site in the BaO layer, O(4), and two inequivalent sites in the CuO_2 planes, O(2) and O(3). The attention to the chain vacancies over others can be attributed to two factors. First, the full deoxygenation of the chains under reducing conditions suggests that the chain vacancy ought to be energetically preferable. Second, the position of V_O is commonly detected using diffraction-based techniques involving either x rays, neutrons, or electrons. However, owing to their large interaction volume, such techniques are sensitive only when the vacancy concentration is large; and at large concentrations, V_O in YBCO prefers to order in the chains [6]. Both of these factors obscure the behavior of V_O at small concentrations, or low x, where T_c peaks. Nonetheless, there are a few reports of V_O at sites other than the chains. For instance, neutron diffraction studies [7–11] have indicated small vacancy concentrations at the apical site O(4), depending on the annealing process. There have been attempts at atomic-scale characterization of V_O on surfaces of cleaved YBCO crystals having optimal doping using scanning tunneling microscopy (STM) [12–15]. Pan *et al.* [12] observed modulations in the intensity of the BaO surface and attributed them to apical vacancies; however, subsequent STM studies did not find any apical vacancies [14] and concluded that the previously observed modulations were due to electronic ordering in the underlying CuO_2 plane [13]. To summarize, while there is some evidence that apical vacancies can form in YBCO at optimal doping, the results are inconclusive owing to either the low spatial resolution of the characterization techniques or to the sample preparation methods. Furthermore, little is known about the conditions that favor the formation of apical vacancies and their effect on YBCO's structure and properties.

In this paper, we provide direct evidence of apical V_O in optimally doped thin films and single crystals of YBCO by using a combination of aberration-corrected scanning transmission electron microscopy (STEM) and first-principles density-functional-theory (DFT) calculations. Based on DFT

*These authors contributed equally to this work.
†Corresponding authors: jgazqueza@gmail.com
‡Corresponding authors: rmishra@wustl.edu

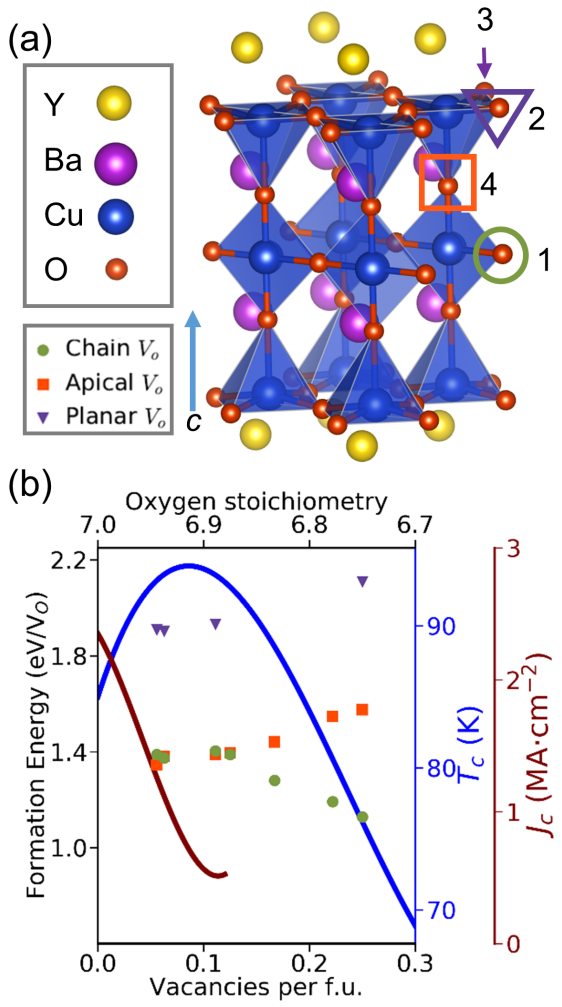

FIG. 1. (a) The atomic structure of fully oxygenated $YBa_2Cu_3O_7$ ($YBCO_7$). The locations of the four possible oxygen vacancies are marked. (b) Oxygen vacancy formation energy as a function of oxygen stoichiometry, using the same colors and symbols as (a). The solid blue line shows T_c, based on experimental data (Ref. [17], while the solid brown line shows J_C (Ref. [2]. O(2) and O(3) are combined because they have nearly identical formation energies.

calculations, we find that isolated apical V_O have a small formation energy, comparable to that of isolated chain V_O, and should exist across the entire doping range. Using atomic-resolution STEM imaging, we show that apical vacancies are most common in the vicinity of $YBa_2Cu_4O_8$ (YBCO-124) intergrowths, which are prevalent stacking faults formed by the inclusion of a second layer of CuO chains. Furthermore, the observed distortions around the apical vacancies in the STEM images match the equivalent DFT-optimized structural distortions, confirming their origin. We find that the apical vacancies modify the electronic structure of adjacent plane Cu atoms, as shown by simultaneously acquired electron energy loss spectra (EELS) in STEM. DFT calculations show that the apical vacancies increase the electron density of the adjacent superconducting CuO_2 planes. Finally, we compare our results with prevalent models of cuprate superconductivity, and consider how apical vacancies might affect YBCO's superconductive properties.

II. RESULTS AND DISCUSSION

To assess the favorability of different V_O in the optimal doping region, we calculated the formation energies (E_{form}) of apical, chain, and planar V_O in YBCO by varying x from 0.05 to 0.25 vacancies per formula unit. We only considered one vacancy type when varying the concentration; interaction of different vacancy types is briefly addressed in the Supplemental Material [16]. For $x < 0.15$, we find that isolated apical O(4) and chain O(1) vacancies have similar E_{form}, as shown in Fig. 1(b). For instance, at $x = 0.06$, E_{form} of an isolated apical and chain V_O is 1.35 and 1.39 eV, respectively, suggesting that the two are likely to exist at similar concentrations. Although a previous work has examined the ordering of chain vacancies in YBCO at higher V_O concentrations using DFT [6], we are not aware of any first-principles studies comparing the stability of isolated apical and chain vacancies. It is not favorable to form vacancies at the planar sites O(2) and O(3), as they have E_{form} of 1.90 and 1.91 eV, respectively, at $x = 0.06$. At higher concentrations, we find that chain vacancy formation benefits from ordering. For instance, for $x = 0.25$, E_{form} of the chain vacancy decreases to 1.13 eV, while it increases for the apical vacancy to 1.58 eV. We find that the lowest energy ordering of chain V_O is an entire chain emptied of oxygen, in agreement with previous experiments [4] and theory [6]. Additional results on V_O ordering and formation energy of apical V_O in other cuprates are included in the Supplemental Material.

We have used STEM annular bright-field (ABF) imaging, which is sensitive to lighter elements [18,19], to identify oxygen vacancies in YBCO samples synthesized by chemical solution deposition; the synthesis and characterization procedures are described in the Supplemental Material. Figure 2(a) shows an ABF image of YBCO. Figure 2(b) shows the same image with its contrast inverted to show the oxygen columns in the BaO layers and the CuO chains with more clarity. We show the intensity trace measured along two BaO layers close to a YBCO-124 stacking fault. While the Ba columns have the same intensity for both layers, the O(4) column closer to the film surface has a lower intensity than the O(4) column farther from the surface, indicating the presence of apical vacancies. We observe a similar intensity difference for pairs of BaO layers several unit cells away from the faults, with the layer closer to the surface consistently having more apical vacancies. Crystallographically, the near and far planes are equivalent, so the asymmetry in vacancy concentration may be due to kinetic factors during the growth process. We have also performed STEM image simulations on DFT-optimized structures containing O(4) vacancies to directly compare with the experimental images. Figure 2(d) shows a simulated contrast-inverted ABF image of a DFT-optimized supercell having 25% V_O in one of the BaO planes. We find good agreement between the simulated and experimental intensity profile changes, confirming the presence of apical V_O.

Apical vacancies are expected to create structural distortions in their vicinity that serve as additional evidence of their presence. We have quantified these distortions from the ABF images by locating the different atomic columns using a center-of-mass refinement method (see the Supplemental Material for details). By measuring the change in various lattice spacings around BaO layers with or without apical V_O,

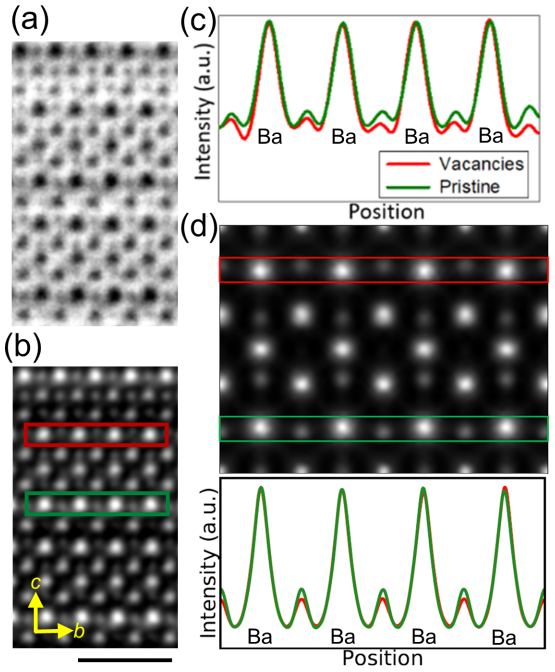

FIG. 2. (a) Raw ABF image of a YBCO thin film with a YBCO-124 intergrowth viewed along the [100] zone axis. (b) The same ABF image with its contrast inverted to show the atomic columns as bright spots. The image has been filtered to reduce the noise. Scale bar: 1 nm. (c) Panel showing two horizontal intensity profiles measured along the BaO planes near to the intergrowth. (d) A simulated contrast-inverted ABF image of a YBCO supercell relaxed with 25% oxygen vacancies in one of the apical planes, marked with a red box, which corresponds to the red intensity trace.

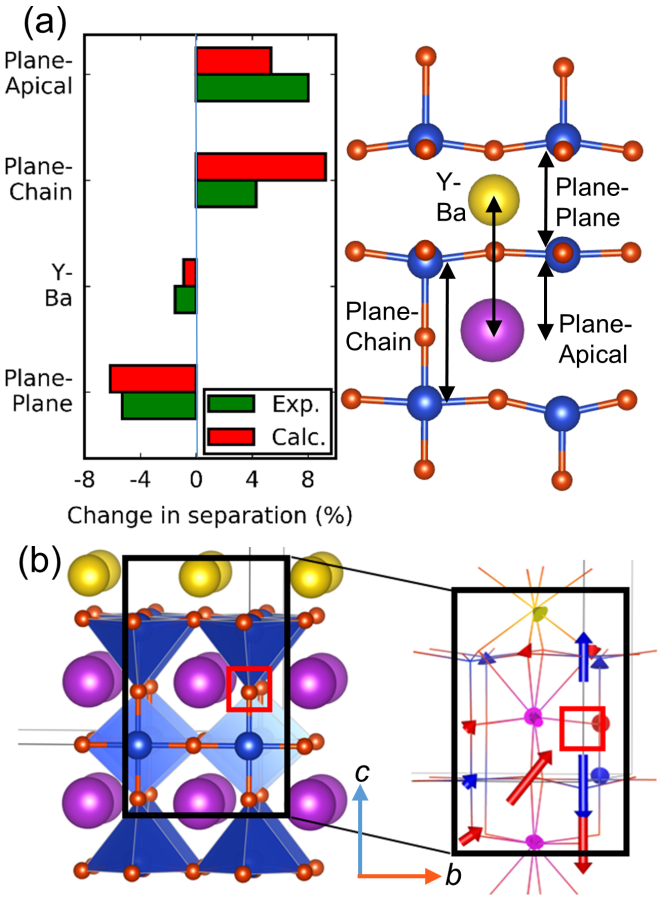

FIG. 3. (a) The change in the interlayer separations for the experimental STEM images and the DFT-calculated YBCO structure with apical vacancies. Each separation is labeled in the schematic. (b) Structural relaxation around an apical V_O as calculated using DFT. The left panel shows the location of the vacancy in the pristine $YBCO_7$, while the right panel is a wireframe of the relaxed structure with vectors showing the atomic displacements. The vectors follow the same color scheme as the atoms; red vectors show O movement, blue Cu, magenta Ba, and yellow Y. The vector length is magnified fivefold for clarity.

we have obtained a detailed real-space map of the vacancy-induced structural distortions. For comparison, we have used DFT to optimize a $3 \times 3 \times 1$ supercell of stoichiometric $YBCO_7$ with one apical vacancy. We show the largest distortions caused by the apical V_O, both in experiments and DFT calculations, in Fig. 3(a). Due to the apical V_O, the spacing along the c axis between Y and Ba is reduced by 1.5% relative to the regions without apical V_O. The planar Cu atom, adjacent to the vacancies, shifts closer to Y, whereas O(2) and O(3) atoms shift in the opposite direction, changing the planar O–Cu–O angle from $165 \pm 2°$ to $176 \pm 2°$. This motion also reduces the interplane Cu–Cu distance by 5.3%, and increases the distance between planar Cu and the remaining apical O(4) in the atomic column by 8 ± 3%. We find excellent agreement between these observed distortions and the calculated distortions, as shown in Fig. 3(b). The calculated apical V_O causes the copper atoms above and below to move away by 0.18 and 0.23 Å, respectively, flattening the in-plane O–Cu–O bond angle from 163° to 175° and buckling the usually straight (180°) chain O–Cu–O angle to 154°. In addition, the adjacent chain oxygen moves towards the vacancy by 0.23 Å.

The presence of apical V_O and the associated distortions affect the local electronic structure of YBCO, as observed from simultaneously acquired EEL spectra. Figure 4(a) compares the fine structure of the O K edge in CuO_2 planes and CuO chains that were acquired from a region of the thin film away from apparent apical V_O. Our results match well with those obtained by Gauquelin *et al.* [20] from a YBCO single crystal that we take as a reference to validate the quality of our EELS measurements. The prepeak of the O K edge is sensitive to the filling of the unoccupied, hybridized O-$2p$ and Cu-$3d$ states, and is observed to shift to higher energies with oxygen vacancies, due to the electron doping [20]. In addition, our observation of the prepeak onset at 527 eV for the CuO chains and 528.5 eV for the CuO_2 planes is consistent with previous results for $YBCO_{6.97}$ single crystals [20], indicating that our thin films have the optimal oxygen concentration. The EELS edge of Cu from chains and planes is provided in the Supplemental Material.

We now show the difference in Cu L and O K edges in the EEL spectra of two superconducting CuO_2 planes with and without adjacent apical V_O in Figs. 4(b) and 4(c), respectively. For the planar O K edge, the most notable difference is the decrease in the intensity of the prepeak in the planes adjacent to the apical V_O. We attribute this to electron doping by the adjacent apical V_O of the previously unoccupied O $2p$ states

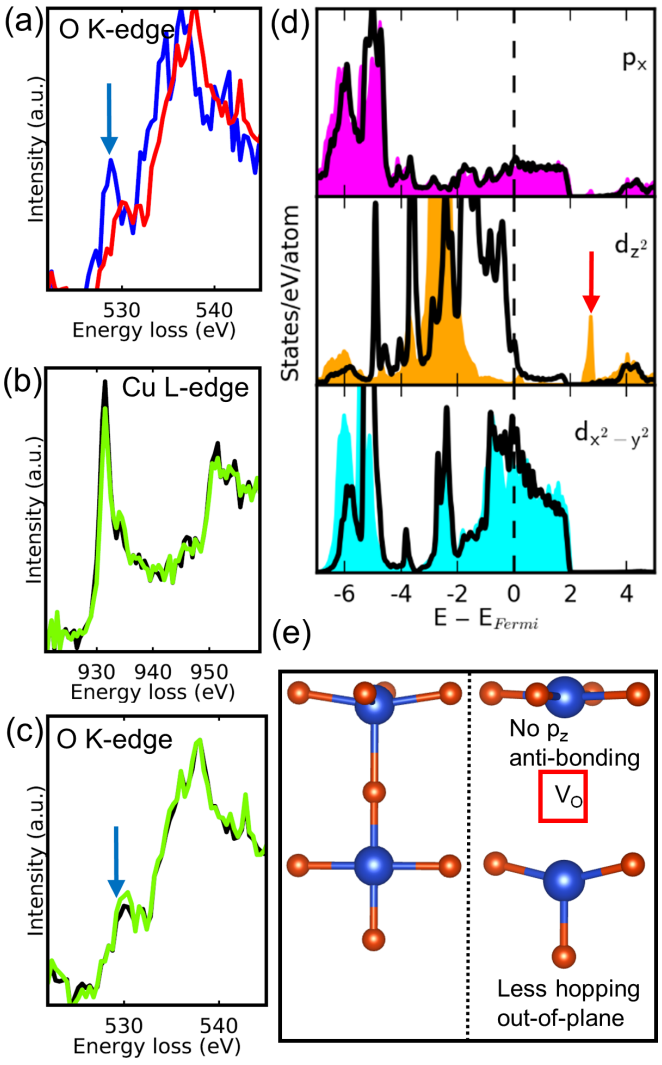

FIG. 4. (a) EELS O *K*-edge spectra obtained from the chain O(1) (blue) and plane O(2), O(3) (red) of optimally doped YBCO thin films. The prepeak is marked with an arrow. (b) Comparison of Cu *L*-edge spectra from CuO_2 planes closer to the film surface (black) with more apical V_O and farther from it with fewer apical V_O (green). (c) Comparison of O *K*-edge spectra from the same CuO_2 planes as in (b). (d) The orbital-projected DOS of the superconducting CuO_2 plane atoms directly adjacent to an apical vacancy. The planar O p_x, Cu $3d_{z^2}$ and Cu $3d_{x^2-y^2}$ states are in magenta, gold, and blue, respectively. The states near 3 eV, highlighted by an arrow correspond to the axial orbital as proposed by Pavarini *et al.* [21]. The black line in the DOS plots corresponds to pristine YBCO, shown for comparison. (e) Schematic of the plane-chain system before and after the apical oxygen is removed.

hybridized with Cu $3d$ in the superconducting planes. The Cu *L*-edge also changes when comparing the two superconducting CuO_2 planes. Notice that the intensity of the Cu L_3-edge (centered at 931.5 eV) increases with apical vacancies, which constitutes a second experimental evidence of an electronic reconstruction. The DFT-calculated electronic density of states (DOS) for the planar Cu and planar O adjacent to an apical V_O are shown in Fig. 4(d), compared with the same atoms in pristine YBCO. The formation of an apical V_O eliminates the overlap between the apical oxygen's $2p_z$ states and the neighboring planar copper's $3d_{z^2}$ states, reducing the bandwidth by ∼2 eV. This interaction is antibonding near the Fermi energy, so the resulting nonbonding Cu $3d_{z^2}$ state drops below the Fermi energy. The remaining planar Cu DOS at the Fermi energy comes from the $3d_{x^2-y^2}$ states, which retain their bandwidth after the apical vacancy formation.

The apical oxygen has been shown to affect the superconducting properties of YBCO. For instance, a recent investigation [22] of the magnetic excitations in cuprates with zero, one, or two apical oxygen per CuO_2 plane concluded that the structure without apical oxygen had the most long-range electron hopping. Likewise, any strain or distortion of the CuO_2 planes is likely to alter the pair condensation energy and its J_C [3]. Hence, we consider the implications of apical V_O.

Pavarini *et al.*, [21] have ascribed an important role to the "axial" molecular orbital, composed of planar Cu $4s$ and $3d_{z^2}$ states antibonding to apical O $2p_z$ states. The axial orbital is above the Fermi energy, and its calculated energy is correlated with T_c; as the axial orbital approaches the Fermi energy, T_c goes up. Increasing the planar Cu–O(4) bond length is predicted to raise T_c by reducing the antibonding contribution to the axial orbital. Removing the apical oxygen is equivalent to a large bond length increase, along with the addition of electrons. It results in the axial orbital, located ∼3 eV above Fermi energy as shown in Fig. 4(d), being entirely composed of Cu $4s$ and $3d_{z^2}$ states. The change may favor in-plane superconductivity, as it has been shown that the single-layer cuprate superconductor having the highest T_c, $HgBa_2CuO_4$, has the most Cu $4s$ character in its axial orbital [21]. However, later studies of the role of apical bonding have not all found the same conclusion. One recent study found no correlation between apical bond length and T_c across many different cuprates, and instead found T_c was correlated with the strength of the bond between the O(4) and the chain Cu [23].

A second well-known model focuses on out-of-plane transport, treating the CuO_2 planes as perfect superconductors and modeling conductivity out of plane as tunneling through a Josephson junction [24]. According to this model, the tunneling barrier between CuO_2 planes is the limiting factor, and anything that shortens the planar Cu–O(4) bond might raise T_c. For example, vacancy-ordered $YBCO_{6.5}$ showed coherent transport near room temperature on optically exciting a phonon mode specific to the Cu–O(4) bond [25,26]. Time-resolved diffraction and theoretical calculations indicated that the excited mode increased planar buckling [26], which ought to reduce in-plane transport but improve out-of-plane transport. According to this model, apical V_O is likely to weaken the out-of-plane superconductivity.

III. CONCLUSION

In summary, we have reported direct observation of apical V_O in optimally doped YBCO. We find that for low vacancy concentrations, isolated apical and chain V_O has similar formation energy. Apical V_O significantly distort the surrounding lattice and the electronic structure of YBCO and are likely to influence its superconductive properties, although the underlying mechanisms of cuprate superconductivity are not yet understood well enough to predict the exact effect. A strategy to understand the role of the apical vacancies could

be to apply a stimulus, such as strain, to stabilize apical V_O over chain V_O and monitor the changes in superconducting transport. Likewise, the association between apical vacancies and stacking faults also need to be investigated. It is clear that future efforts to understand the high-T_c superconductivity of YBCO, need to take into account the role of apical V_O on an equal footing as the doping by chain V_O.

ACKNOWLEDGMENTS

This work was partially supported by the National Science Foundation (NSF) Grant No. DMR-1806147 (S.T.H., R.M.). Computations in this work benefited from the use of the Extreme Science and Engineering Discovery Environment (XSEDE), which is supported by NSF Grants No. ACI-1053575 and No. ACI-1548562. B.M, J.G., T.P., and X.O acknowledge financial support from the Spanish Ministry of Science Innovation and Universities through the 'Severo Ochoa' Programme for Centres of Excellence in R&D (SEV-2015-0496), and the COACHSUPENERGY project (SUMATE - RTI2018-095853-B-C21, co-financed by the European Regional Development Fund). They also thank the European Union for its support under the ULTRASUPERTAPE project (ERC-2014-ADG-669504), and COST Action NANOCOHYBRI (CA16218), and from the Catalan Government under 2017-SGR-1519 and XRE4S. J.G. also acknowledges the Ramon y Cajal program (RYC-2012-11709). STEM imaging and analysis at 200 kV was sponsored by the US Department of Energy (DOE), Office of Science, Basic Energy Sciences, Materials Sciences and Engineering Division, and STEM imaging at 100 kV was conducted at the Center for Nanophase Materials Sciences, which is a DOE Office of Science User Facility (J.-C.I.).

This work has been partially supported by US DOE Grant No. DE-FG02-13ER41967. ORNL is managed by UT-Battelle, LLC, under Contract No. DE-AC05-00OR22725 for the US DOE. The US Government retains and the publisher, by accepting the article for publication, acknowledges that the United States Government retains a non-exclusive, paid-up, irrevocable, worldwide license to publish or reproduce the published form of this manuscript, or allow others to do so, for US Government purposes. The Department of Energy will provide public access to these results of federally sponsored research in accordance with the DOE Public Access Plan [27].

[1] R. J. Cava, B. Batlogg, K. M. Rabe, E. A. Rietman, P. K. Gallagher, and L. W. Rupp, Physica C **156**, 523 (1988).
[2] E. F. Talantsev, N. M. Strickland, S. C. Wimbush, J. G. Storey, J. L. Tallon, and N. J. Long, Appl. Phys. Lett. **104**, 242601 (2014).
[3] G. Deutscher, APL Mater. **2**, 096108 (2014).
[4] J. D. Jorgensen, M. A. Beno, D. G. Hinks, L. Soderholm, K. J. Volin, R. L. Hitterman, J. D. Grace, I. K. Schuller, C. U. Segre, K. Zhang, and M. S. Kleefisch, Phys. Rev. B **36**, 3608 (1987).
[5] J. Gazquez, R. Guzman, R. Mishra, E. Bartolomé, J. Salafranca, C. Magén, M. Varela, M. Coll, A. Palau, S. M. Valvidares, P. Gargiani, E. Pellegrin, J. Herrero-Martin, S. J. Pennycook, S. T. Pantelides, T. Puig, and X. Obradors, Adv. Sci. **3**, 1500295 (2016).
[6] A. Filippetti, G. M. Lopez, M. Mantega, and V. Fiorentini, Phys. Rev. B **78**, 233103 (2008).
[7] J. D. Jorgensen, S. Pei, P. Lightfoor, H. Shi, A. P. Paulikas, and B. W. Veal, Physica C **167**, 571 (1990).
[8] J. D. Jorgensen, H. Shaked, D. G. Hinks, B. Dabrowski, B. W. Veal, A. P. Paulikas, L. J. Nowicki, G. W. Crabtree, W. K. Kwok, L. H. Nunez, and H. Claus, Physica C **153–155**, 578 (1988).
[9] A. P. Shapovalov, M. B. Yu, A. I. Ruban, G. G. Gridneva, V. S. Melnikov, and N. P. Pshentsova, Supercond. Sci. Technol. **5**, 283 (1992).
[10] J. C. Cheang Wong, C. Ortega, J. Siejka, I. Trimaille, A. Sacuto, L. M. Mercandalli, and F. Mayca, J. Alloys Compd. **195**, 675 (1993).
[11] J. L. MacManus-Driscoll, J. A. Alonso, P. C. Wang, T. H. Geballe, and J. C. Bravman, Physica C **232**, 288 (1994).
[12] S. H. Pan, E. W. Hudson, and J. C. Davis, Rev. Sci. Instrum. **70**, 1459 (1999).
[13] T. Nishizaki, M. Maki, and N. Kobayashi, J. Phys. Chem. Solids **69**, 3014 (2008).
[14] T. Nishizaki, K. Shibata, M. Maki, and N. Kobayashi, J. Low Temp. Phys. **131**, 931 (2003).
[15] M. Maki, T. Nishizaki, K. Shibata, and N. Kobayashi, J. Phys. Soc. Jpn. **70**, 1877 (2001).
[16] See Supplemental Material at http://link.aps.org/supplemental/10.1103/PhysRevMaterials.3.114806 for experimental and computational details, as well as additional STEM-EELS data and DFT results.
[17] R. Liang, D. A. Bonn, and W. N. Hardy, Phys. Rev. B **73**, 180505(R) (2006).
[18] R. Ishikawa, E. Okunishi, H. Sawada, Y. Kondo, F. Hosokawa, and E. Abe, Nat Mater **10**, 278 (2011).
[19] J. Gazquez, M. Stengel, R. Mishra, M. Scigaj, M. Varela, M. A. Roldan, J. Fontcuberta, F. Sanchez, and G. Herranz, Phys. Rev. Lett. **119**, 106102 (2017).
[20] N. Gauquelin, D. G. Hawthorn, G. A. Sawatzky, R. X. Liang, D. A. Bonn, W. N. Hardy, and G. A. Botton, Nat. Commun. **5**, 4275 (2014).
[21] E. Pavarini, I. Dasgupta, T. Saha-Dasgupta, O. Jepsen, and O. K. Andersen, Phys. Rev. Lett. **87**, 047003 (2001).
[22] Y. Y. Peng, G. Dellea, M. Minola, M. Conni, A. Amorese, D. Di Castro, G. M. De Luca, K. Kummer, M. Salluzzo, X. Sun, X. J. Zhou, G. Balestrino, M. Le Tacon, B. Keimer, L. Braicovich, N. B. Brookes, and G. Ghiringhelli, Nat. Phys. **13**, 1201 (2017).
[23] S. Kim, X. Chen, W. Fitzhugh, and X. Li, Phys. Rev. Lett. **121**, 157001 (2018).
[24] P. W. Anderson, Science **279**, 1196 (1998).
[25] S. Kaiser, C. R. Hunt, D. Nicoletti, W. Hu, I. Gierz, H. Y. Liu, M. Le Tacon, T. Loew, D. Haug, B. Keimer, and A. Cavalleri, Phys. Rev. B **89**, 184516 (2014).
[26] R. Mankowsky, A. Subedi, M. Forst, S. O. Mariager, M. Chollet, H. T. Lemke, J. S. Robinson, J. M. Glownia, M. P. Minitti, A. Frano, M. Fechner, N. A. Spaldin, T. Loew, B. Keimer, A. Georges, and A. Cavalleri, Nature (London) **516**, 71 (2014).
[27] http://energy.gov/downloads/doe-public-access-plan.